RSC Advances

PAPER

Cite this: *RSC Adv.*, 2015, **5**, 8622

Rapid construction of TiO_2 aggregates using microwave assisted synthesis and its application for dye-sensitized solar cells

Xuyang Wang,[a] Jianjun Tian,*[a] Chengbin Fei,[b] Lili Lv,[a] Yajie Wang[b] and Guozhong Cao*[bc]

Received 26th September 2014
Accepted 15th December 2014

DOI: 10.1039/c4ra11266k

www.rsc.org/advances

Hierarchical TiO_2 nanocrystallite aggregates, composed of ~10 nm nanocrystallites, with a size of ~500 nm have been synthesized by a microwave assisted method at 150 °C in a short time (~10 minutes) as the photoanode of dye-sensitized solar cells (DSCs). Ethanol and $TiCl_4$ are selected as the solvent and titanium precursor, respectively. The rapid heating rate and superheating/"hot spots" of the reaction system under microwave irradiation result in a large amount of nuclei instantly, which leads to the formation of a great deal of clusters. Moreover, the clusters that grow up rapidly are assembled into TiO_2 nanocrystallite aggregates. The TiO_2 aggregates show better light scattering property, larger specific surface area and higher dye-loading compared to the commercial P25 TiO_2 nanoparticles. In comparison with DSC based P25 photoanode, the short current density (J_{sc}) and dye-loading of DSC based the as-synthesized TiO_2 aggregates photoanode increase by 33% and 62%, respectively. As a result, the PCE of the DSC is up to 7.64%, and the TiO_2 aggregates obtained by microwave assisted synthesis are a promising and potential candidate for DSCs.

1. Introduction

Mesoporous oxide semiconductors (MOS) have been regarded as an attractive material for solar cells, solar fuel, photo catalysts and energy storage devices due to their high surface area, and excellent photoelectric and electrochemical properties.[1,2] Among various MOSs, anatase titanium dioxide (TiO_2) has been studied widely in dye-sensitized solar cells (DSCs), which were first reported by Oregan and Grätzel in 1991.[3] Because of the low cost of the production, DSCs have attracted certain attention in the field of photovoltaics. The MOS TiO_2 film is one of the key components in such cells, which plays an important role in the adsorption of dyes and electronic transmission.[4–10] Recently, power conversion efficiency (PCE) (as high as 13%) in DSCs device based on MOS TiO_2 film has been achieved using a molecularly engineered porphyrin dye, coded SM315, under full sun illumination (AM 1.5G, 100 mW cm^{-2}).[11]

A lot of research for efficient DSC devices has been conducted for the synthesis of a variety of TiO_2 nanostructures in the forms of wires, tubes, spheres, rods, sheets, belts, flowers and trees.[12–16] To increase the electron mobility, one-dimensional (1D) TiO_2 nanostructures, such as nanotube arrays and single-crystalline nanowire arrays, have been studied as photoanodes for DSCs.[12] However, as expected, DSCs based on 1D structures have not reached high conversion efficiency due to the much small surface area for dye adsorption.[17] 3D hierarchical nanostructures can offer larger surface areas for dye adsorption while simultaneously enhancing light scattering for efficient photon harvesting, and thereby improving power conversion efficiency.[16–19] The aggregate structure consisting of primary nanocrystallites can provide both large specific surface area and a light scattering effect so as to enhance the performance of DSCs.[19–25] Previous studies have shown that photoanodes with hierarchical aggregates structure are promising for highly efficient DSCs.

In the last few decades, many methods, such as sol–gel,[26] hydrothermal,[27] solvothermal[28] and template[29] approaches, have been used to synthesize TiO_2 nanostructures. Hydrothermal and solvothermal methods have been frequently used because they are capable of providing the desired size and structure of TiO_2 nanocrystals by controlling the temperature, duration, and concentration of the reaction. However, drawbacks like the complex and time-consuming process have been pointed out for hydrothermal and solvothermal methods. The high cost and low productivity of the hydrothermal and solvothermal methods are considered as a big hindrance for their applications in DSCs. There is growing need to develop a fast and high productivity synthesis method to obtain TiO_2 nanocrystals for their application in DSCs. Compared with

[a]*Advanced Materials and Technology Institute, University of Science and Technology Beijing, 100083, China. E-mail: tianjianjun@mater.ustb.edu.cn*

[b]*Beijing Institute of Nanoenergy and Nanosystems, Chinese Academy of Sciences, 100083, China*

[c]*Department of Materials and Engineering, University of Washington, Seattle, WA 98195-2120, USA. E-mail: gzcao@u.washington.edu*

hydrothermal and solvothermal methods, the microwave assisted synthesis offers rapid processing speed, homogeneous heating and simple control of processing conditions, and thus has attracted much attention in the last few years.[30] Thus, microwave assisted synthesized TiO_2 nanocrystallites have shown their potentials as photoanodes for DSCs in recent studies.[31–35] For example, Dar *et al.*[31] synthesized TiO_2 nanoparticles (~7 nm) and nanospheres (100–400 nm) of TiO_2 from the same precursor using a microwave assisted approach. After using these nanostructures as a photoanode in DSCs, a modest yet appreciable efficiency of 6.5% was achieved. Manseki *et al.*[32] prepared the highly crystallized TiO_2 nanorods by the microwave assisted method to construct a photoanode for DSCs. Shen *et al.*[35] reported pure anatase TiO_2 nanoparticles with a size of about 20 nm, which were obtained by the microwave assisted method for DSCs. PCE of the solar cells based nanoparticles was up to 7.7%. Thus, the microwave assisted synthesis is considered as a facile, energy-saving and mass production scalable approach to replace hydrothermal and solvothermal processes without sacrificing the photovoltaic performances of DSCs.

In this study, microwave assisted synthesis has been taken to synthesize hierarchically TiO_2 nanocrystallite aggregates. Ethanol and $TiCl_4$ are selected as the solvent and titanium precursor, respectively. The nearly spherical TiO_2 aggregates with a size of ~500 nm were composed of ~10 nm nanocrystallites, which show better light scattering property, larger specific surface area and higher dye-loading than those of the commercial P25 TiO_2 nanoparticles. In comparison with P25 TiO_2 photoanode, the short current density (J_{sc}) and dye-loading of the DSC-based as-synthesized aggregates TiO_2 photoanode increased by 33% and 62%, respectively. As a result, the PCE of the DSC reaches 7.64%. The possible mechanisms for such enhancement in the power conversion efficiency have been discussed.

2. Results and discussion

TiO_2 nanocrystallites are prepared by microwave assisted synthesis at 150 °C in only 10 minutes in this paper. Fig. 1 shows the XRD pattern of the as-synthesized dry solid powder by the microwave assisted method. XRD peaks can be indexed to the anatase structure of standard TiO_2 (JCPDS 21-1272). Within the detection limit of XRD, no peak characteristic of any impurity is found in the as-synthesized powder, indicating the as-synthesized product is a pure anatase TiO_2 phase. The SEM images of as-synthesized TiO_2 samples are presented in Fig. 2(a) and (b). The presence of the TiO_2 nanocrystallite aggregates assembled by agglomerated nanoparticles with sizes of ~10 nm was observed. The TiO_2 nanocrystallite aggregates possess a size of ~500 nm in diameter and show nearly spherical morphology. The mesoporous film prepared by TiO_2 aggregates can serve as organic dyes scaffold to collect and transfer the excited electrons from the dyes. This film is much more porous with voids as large as several micrometers, which facilitates dyes to permeate into the interior of the film. In addition, the aggregates contain a large amount of nanoparticles, which leads to increase in the specific surface to absorb much more dye. Fig. 2(c) and (d) show the HRTEM images of the TiO_2 aggregates. It can be seen that the nanocrystallite cluster is assembled with single crystals with a size of ~5 nm, corresponding to the anatase (101) facet (see FFT patterns). This, the crystal growth is favourable along the [101] direction during the microwave assisted synthesis process.

In this study, $TiCl_4$ and ethanol are selected as the titanium precursor and solvent, respectively. $TiCl_4$ is widely used for titania synthesis and is very reactive to water or oxygen, forming titanium hydroxide. It should be noted that the reaction in ethanol is very slow at room temperature, and reaction temperatures of 80–150 °C are generally required to obtain reasonable rates and crystalline products.[36] Fig. 3(a) displays the La-Mer model for nucleation and growth kinetics of nanoparticles.[37] The process of formation of nanocrystals is classically divided into two events: nucleation and growth. When supersaturation is relieved by the formation of nuclei, the system enters the growth stage, in which no additional nuclei are formed but only existing clusters grow larger.[36–38] The nucleation and growth processes can be influenced by heating rate. As for microwave assisted synthesis, the mixture is heated to the reaction temperature (~150 °C) in a very short time (1–3 minutes), which leads to the formation of a large amount of crystal nuclei. Once the nucleation starts, the reaction system immediately enters the growth process and the nuclei grow rapidly. The overall processes containing nucleation and growth are drastically shorted by rapid heating of the microwave method. Fig. 3(b) is a schematic illustration of the formation process for as-synthesized TiO_2 aggregates by microwave assisted method. The microwave nucleated precursors had a higher population of nuclei with smaller sizes than the precursors nucleated by conventional heating.[39] During the transient stage of nucleation, many small crystals easily touch together to be assembled into clusters due to their high surface energy. The rapid heating rate and superheating/"hot spots" of the reaction system under microwave irradiation result in a rapidly increased reaction rate.[39] Thus, the clusters grow rapidly, and are assembled into TiO_2 nanocrystallite aggregates.

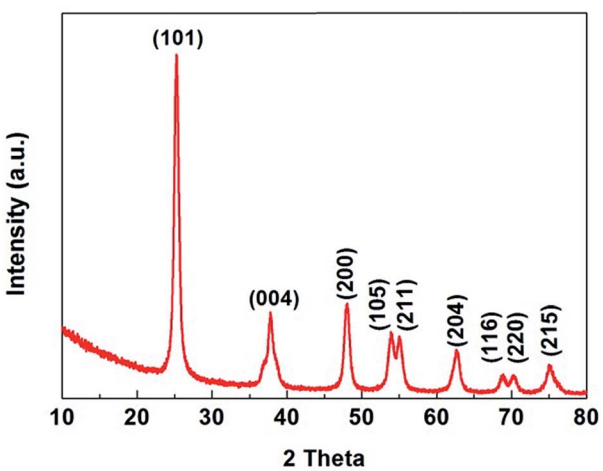

Fig. 1 XRD pattern of the as-synthesized TiO_2 powder by microwave assisted method.

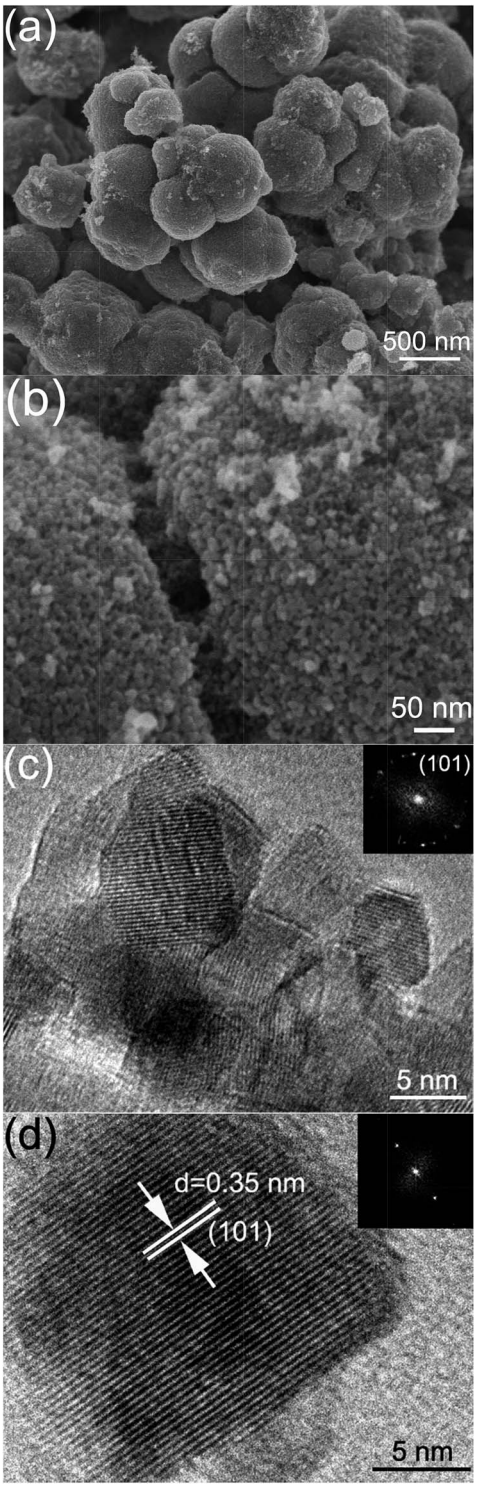

Fig. 2 SEM images (a and b) and (c and d) HRTEM images of as-synthesized TiO_2 aggregates, inset showing the fast Fourier transform (FFT) diffraction pattern.

Light scattering is an important cause for increase in the absorbance of incident photons for the enhancement of photo-generated current. Efficient light scattering is necessary for high performing photoanodes of DSCs.[19] Normally, when light encounters an object, according to the laws of reflection and refraction, the radiation may either propagate in the forward direction, which gives rise to refraction and absorption, or propagate in the backward direction, which causes reflection.[40] Thus, diffuse reflectance and transmittance data can reveal the extent to which incident light is scattered by particles in the photoanodes and how much the incident light passes through the photoanodes without being scattered.[41] The ideal light scattering properties of a photoanode should be a high diffuse reflectance and low diffuse transmission. Fig. 4(a) and (b) show the diffuse reflection and transmittance spectra curves of P25 TiO_2 nanoparticles (NPs) and TiO_2 aggregate films without sensitization. It can be seen that the diffuse reflectance of TiO_2 aggregates is much stronger than that of TiO_2 NPs in the 400–800 nm range, which is the main wavelength range dye used in DSCs to capture the photons effectively. In addition, the diffuse transmittance of TiO_2 aggregate film is much weaker than that of TiO_2 NP film, indicating that there are more photons trapped in the aggregate film. Fig. 4(c) shows a schematic illustration of the effect of the aggregates on the light scattering. The results can be attributed to the strong scattering of the aggregates, which makes the incident light reflect directly back towards the nanoparticles. As a result, incident light could be scattered more efficiently by the ZnO aggregates synthesized by the microwave assisted method. Thus, the photocurrent and PCE of devices based on TiO_2 aggregates film could be increased by the enhanced light scattering.

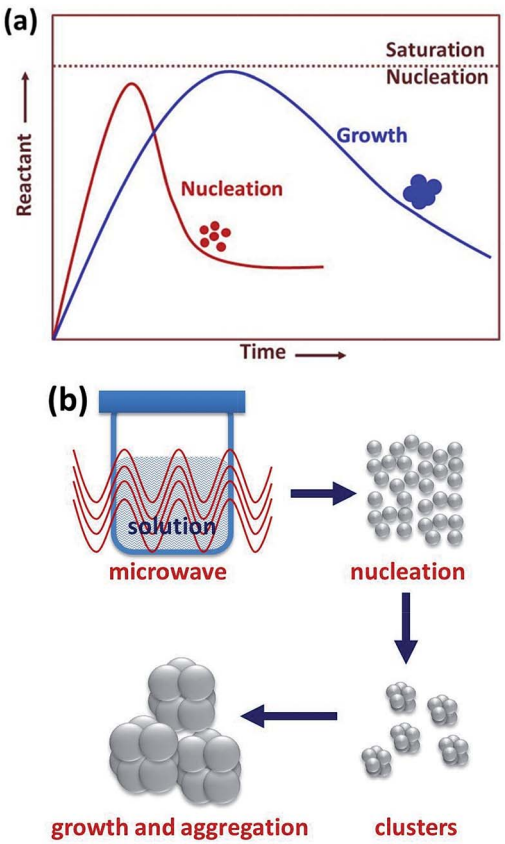

Fig. 3 (a) La-Mer model for nucleation and growth kinetics of nanoparticles and (b) schematic illustration of the TiO_2 aggregate formation process.

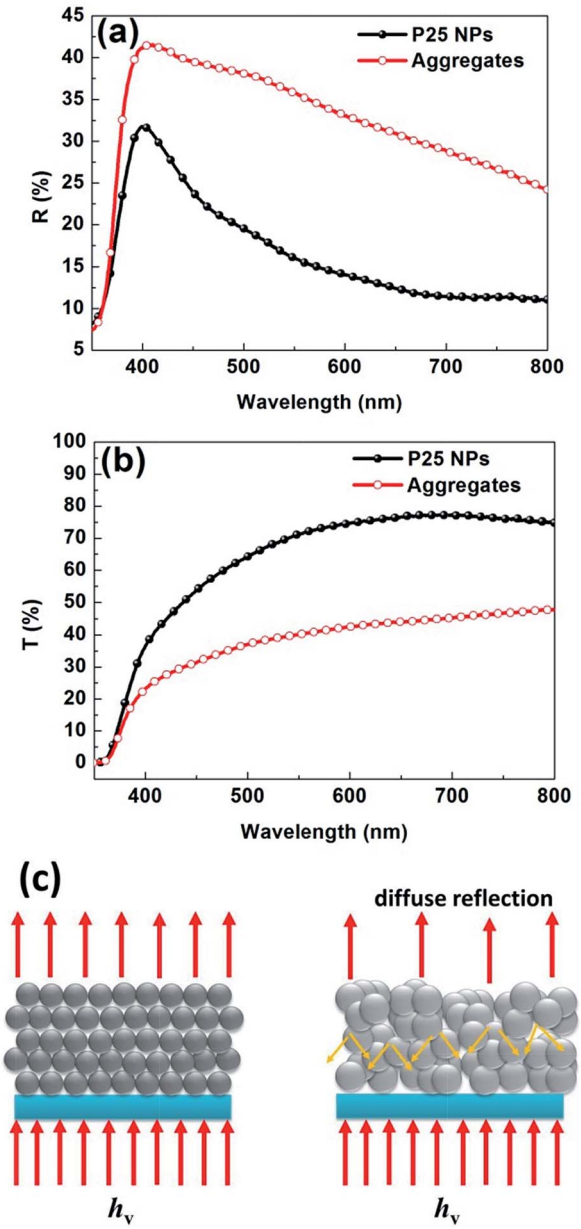

Fig. 4 Diffuse reflectance (a) and transmittance spectra curves (b) of P25 nanoparticle TiO_2 film and TiO_2 aggregate film, and (c) schematic illustration of the effect of the aggregates on light scattering.

To further study the light scattering effects of the different structural TiO_2 films, the "relative diffuse reflectance (R_r)" and "relative diffuse transmittance (T_r)" were proposed to investigate the light capture of the photoanodes with the loading of N719 dye in the range from 350 nm to 800 nm. R_r and T_r can be calculated from the measured diffuse reflectance and diffuse transmittance using the following equations:[19]

$$R_r = \frac{\int_{\lambda_1}^{\lambda_2} I_\lambda R_\lambda d\lambda}{\int_{\lambda_1}^{\lambda_2} I_\lambda d\lambda} \quad (1)$$

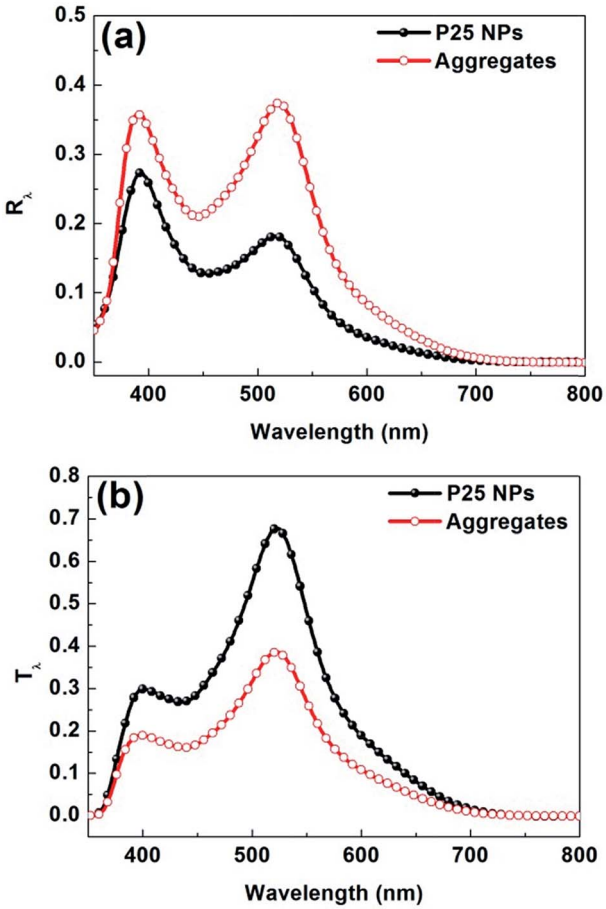

Fig. 5 Relative diffuse reflectance (a) and (b) relative diffuse transmittance curves of P25 nanoparticle TiO_2 film and TiO_2 aggregate film.

$$T_r = \frac{\int_{\lambda_1}^{\lambda_2} I_\lambda T_\lambda d\lambda}{\int_{\lambda_1}^{\lambda_2} I_\lambda d\lambda} \quad (2)$$

where R_λ and T_λ are diffuse reflectance and diffuse transmittance at the certain wavelength, and are shown in Fig. 4(a) and (b). I_λ is the normalized absorption spectra intensity of N719 dye. The λ_1 to λ_2 is corresponding to 350 nm to 800 nm in this study. The results are shown in Fig. 5(a) and (b), indicating that the TiO_2 aggregate film shows higher R_r and lower T_r than those of TiO_2 NP film in the 400–700 nm range, which agrees with the results in Fig. 4(a) and (b). Therefore, the TiO_2 aggregate film synthesized by the microwave assisted method has better light scattering than P25 nanoparticle film.

Fig. 6(a) shows the nitrogen sorption isotherms of P25 and aggregate TiO_2 powders. The detailed surface properties and dye loading are listed in Table 1. It can be seen that the TiO_2 nanocrystallite aggregates have a much higher BET surface area (86.9 $m^2\ g^{-1}$) than the P25 nanoparticles (53.5 $m^2\ g^{-1}$). However, the pore volume (0.17 mL g^{-1}) and average pore size (7.05 nm) are lower than those of P25 nanoparticles (0.20 mL g^{-1} and 14.72 nm). The possible cause is that the size

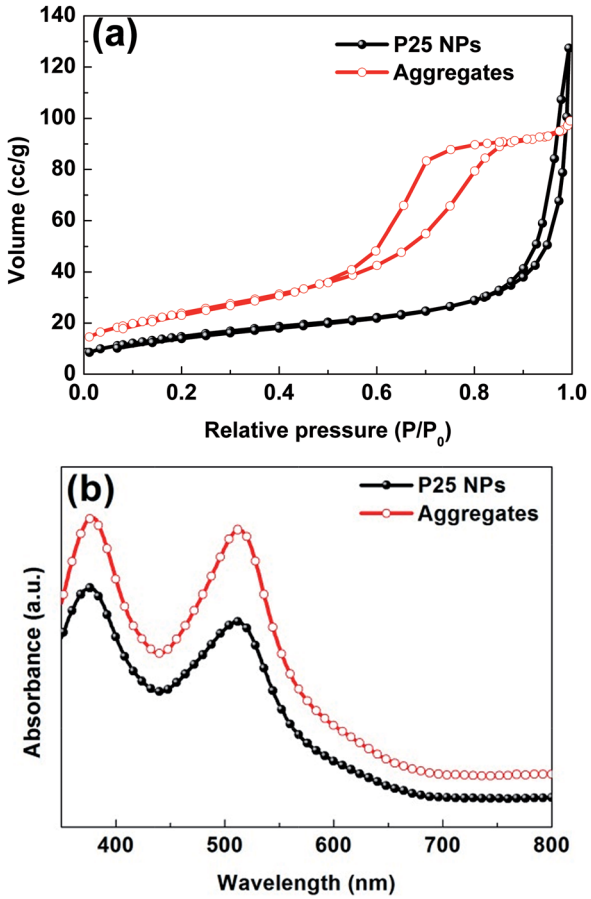

Fig. 6 (a) Nitrogen sorption isotherms of P25 and aggregated TiO_2 powders, and (b) UV-vis absorption spectra of the dye (N719) desorbed from the TiO_2 films.

Table 1 Surface properties and dye loading of different films

Parameters	P25	Aggregates
BET surface area ($m^2\ g^{-1}$)	53.53	86.90
Pore volume (mL g^{-1})	0.20	0.17
Average pore size (nm)	14.72	7.05
Dye-loading (10^{-7} mol cm^{-2})	1.49	2.42

of nanocrystallites within the aggregates (~10 nm as shown in Fig. 2) is smaller than that of P25 nanoparticles (~20 nm as shown in the previous work[21]). The average pore size of the aggregates is calculated using the Barrett–Joyner–Halenda (BJH) method based on the nanocrystallites within the aggregates. However, there are a lot of porous channels among the aggregates that facilitate the dye molecules to penetrate into the interior of the mesoporous films. Although the low pore volume is not good for the dye loading, the difference value (0.03 mL g^{-1}) between the aggregates and P25 is very small, which has little effect on the dye loading of the films. Thus, the dye adsorption of the films is mainly dependent on the specific surface area and surface roughness of the mesoporous films. In order to measure the UV-vis absorption spectra of the dye (N719) absorbed within the films, the dye was desorbed by a 0.5 M NaOH solution in water and ethanol (1 : 1, v/v). The absorption spectra in the visible region of both the P25 and aggregates samples are shown in Fig. 6(b). The calculated amount of dye adsorbed per unit area is 2.42×10^{-7} mol cm^{-2} for the aggregates sample and 1.49×10^{-7} mol cm^{-2} for the P25 nanoparticles sample as shown in Table 1. The aggregates sample displays a higher absorption than the P25 sample, which is consistent with the result of the specific surface areas. Except for the specific surface area, the surface roughness of the mesoporous film is also an important factor for the dye loading. The surface roughness factors for both films can be calculated using the following equation:[42]

$$\mathrm{SRF} = \Gamma_{\mathrm{area}} \times N_{\mathrm{A}} \times A_{\mathrm{dye}} \quad (3)$$

where N_A is Avogadro's number, Γ_{area} is the number of attached dye molecules (mol cm^{-2}), and A_{dye} is the surface area of the dye molecule (assumed to be 10^{-14} nm^2). By calculating the SRF value for P25 is 894, whereas that of the aggregates is 1452. The higher surface roughness of the film is, the more amount of dye loading is.

To further understand the effect of the structure of the photoanodes on the photon-to-current conversion, the incident photon-to-current conversion efficiency (IPCE) spectra have been measured for DSCs with different photoanodes in the range of wavelengths from 400 to 800 nm as shown in Fig. 7. Maximum IPCE of DSC based on aggregates photoanode reaches 65% at 530 nm (the region of maximum light absorption by N719), which is enhanced by ~30% compared to the maximum IPCE of 50% at 530 nm for DSC based on P25 photoanode. IPCE is substantially improved from visible to the near infrared radiation region 750 nm. Thus, the improvement of IPCE of DSC assembled by the aggregates is mainly derived from the enhancement of the diffuse reflectance and light absorbance.

The measurement of electrochemical impedance spectroscopy (EIS) has been carried out to study the charge transfer property in the DSCs based on the different photoanodes. Fig. 8 shows the impedance spectra of the DSCs measured under

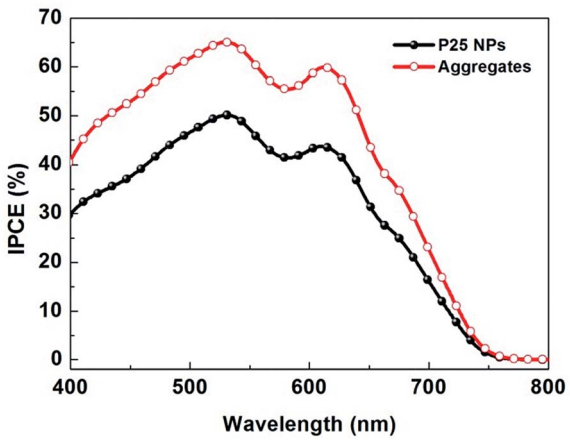

Fig. 7 Incident photon-to-current conversion efficiency (IPCE) spectra of the DSCs with different photoanodes.

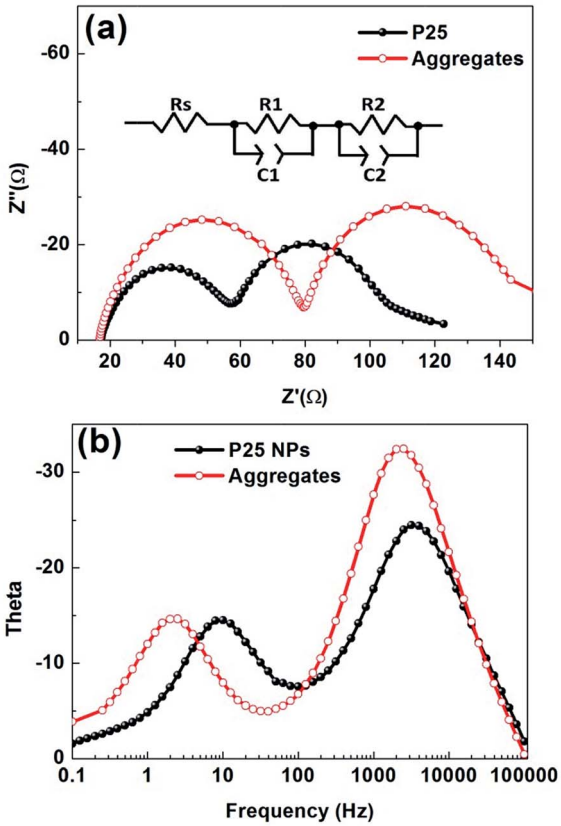

Fig. 8 (a) Nyquist plot and (b) Bode plot of DSCs based on the different photoanodes under dark conditions.

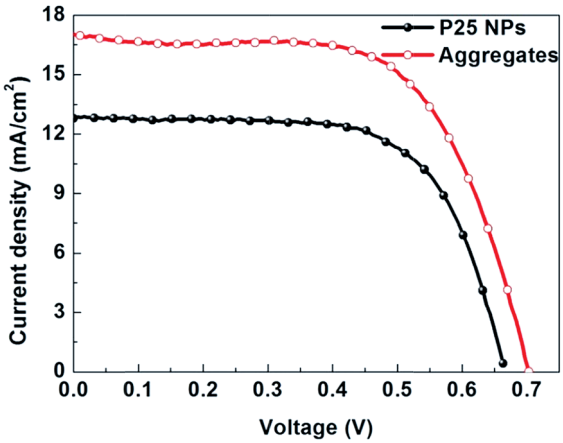

Fig. 9 *J–V* curves of DSCs with different photoanodes.

Table 2 Photovoltaic properties of DSCs with different photoanodes

Samples	V_{oc} (V)	J_{sc} (mA cm^{-2})	FF	PCE (%)
P25	0.66	12.79	0.66	5.57
Aggregates	0.70	17.05	0.64	7.64

forward bias (−0.7 V) under dark condition. In Fig. 8(a), the two semicircles correspond to the resistances of electron diffusion (R_1), and charge transfer (R_2), respectively, at the TiO_2/electrolyte interface.[43] It can be seen that both R_1 and R_2 of DSC based on aggregates are higher those of the DSC based P25 NPs. The higher R_1 of the aggregates photoanode is attributed to the longer path of electron diffusion in the aggregate structure, which is not beneficial to the photo-current (J_{sc}). However, R_2 is considered as the charge transfer resistance.[19,43] A larger value of R_2 indicates less surface charge recombination at the sensitized TiO_2/electrolyte interface, which facilitates the transfer and collection of electrons. In addition, the electron lifetime (τ_n) in the aggregates photoanode is longer than that in P25 photoanode according to Fig. 8(b) ($1/2\pi f_{max}$).[44] The main reason is also ascribed to the decrease of surface charge recombination.

Fig. 9 shows the *J–V* curves for DSCs measured under the illumination of one sun (AM 1.5, 100 mW cm^{-2}). The detailed performance parameters of DSCs based on the different photoanodes are shown in Table 2, where it is obvious that DSCs based on the TiO_2 aggregates prepared by microwave assisted synthesis exhibit high performance: open voltage (V_{oc}) of 0.70 V, short current density (J_{sc}) of 17.05 mA cm^{-2}, fill factor (FF) of 0.64, and PCE of 7.64%. Compared to the P25 nanoparticles, J_{sc} of DSC based on the TiO_2 aggregates increased from 12.79 mA cm^{-2} to 17.05 mA cm^{-2}. As discussed above, the larger surface, higher surface roughness and the stronger scattering of the aggregates leads to the higher dye-loading, more absorbance of the incident photons and higher IPCE, which are the primary causes for the enhancement of photocurrent. In addition, the DSC based on the TiO_2 aggregates shows a little better V_{oc} (0.70 V) than that of the device based on P25 nanoparticles (0.66 V). This possibly due to the difference in the band-gap structure of the aggregates and P25 nanoparticles. As is well known, the maximum value of V_{oc} is determined by the difference between the quasi Fermi level in TiO_2 under illumination and the oxidation potential of the electrolyte.[45] For n-type semiconductor TiO_2, the quasi Fermi level is close to the conduction band.[46] The commercial P25 nanoparticles are composed of 71 wt% anatase and 29 wt% rutile nanoparticles, while the aggregate is the pure anatase phase. The band-gap of anatase (~3.2 eV) is a little higher than that of the rutile (~3.0 eV), which results in the increase of V_{oc} of the aggregates in comparison with the P25 nanoparticles. In addition, EIS results have showed that the high recombination resistance of DSC based on the aggregates is beneficial to the enhancement of V_{oc} because of the decrease of the surface charge recombination.

3. Experimental

3.1 Synthesis of TiO_2 aggregates

TiO_2 aggregates were synthesized through the microwave assisted method. First of all, 0.5 mL titanium tetrachloride ($TiCl_4$) was dissolved in 14 mL ethanol with continuous stirring to form a homogeneous solution in air. The container with the mixture was moved into the microwave reaction device CEM Discover microwave system. The reaction parameters were set as follows: temperature of 150 °C, pressure of 300 Pa, power of

200 W, and time of 10 min. The synthesized precipitate was separated by centrifugation at 6000 rpm for 10 min and rinsed 3 times using ethanol.

3.2 Preparation of the photoanodes

The as-synthesized TiO_2 powder/P25 powder, ethyl cellulose and α-terpineol were combined with ethyl alcohol in a specific proportion to make the paste as reported in a previous study.[47] The paste was then coated on a fluorine-doped tin oxide (FTO) glass substrate *via* the doctor blading method. The as received TiO_2 films underwent a sintering process in air as follows: 125 °C for 30 min and at 500 °C for 30 min at a heating speed of 5 °C min^{-1} to get mesoporous films. The thickness of the sintered films is 15–20 μm. The TiO_2 films were immersed in 0.5 mM N719 ethyl solution for 24 h at room temperature in the dark.

3.3 Characterization

Scanning electron microscopy (SEM, JSM-7000) and transmission electron microscopy (TEM, Tecnai G2 F20) were used with the purpose of characterizing the morphology of the TiO_2 aggregates. The crystal structures of the TiO_2 aggregates were tested by X-ray diffraction (XRD) on an X'Pert PROS (Philips Co.) with a radiation of Cu-Kα (λ = 0.54060 Å). N_2 adsorption–desorption isotherms were recorded on ASAP2020 instrument (Micromeritics Co.), and the specific surface areas (S_{BET}) were calculated using the BET equation. The desorption isotherm was used to determine the pore size distribution using the Barrett–Joyner–Halenda (BJH) method. The concentration of desorbed dye in film was calculated from UV-vis absorption spectra (UV-3600, Shimadzu). The electrochemical impedance spectroscopy (EIS) measurements were also performed with the electrochemical workstation (Zahner, Zennium). The photovoltaic performance of DSCs was measured under a solar simulator (Oriel Sol 3A Solar Simulator, 94063A, Newport Stratford Inc.), equipped with a 300 W xenon lamp (Newport) and a Keithley digital source meter (Keithley, 2400) controlled by Testpoint software. The properties of the solar cells were tested under AM 1.5 simulated sunlight with an output power density of 100 mW cm^{-2}.

4. Conclusions

The nearly spherical TiO_2 aggregates, composed of ~10 nm nanocrystallites, with a size of ~500 nm have been prepared by a microwave assisted method at 150 °C for 10 minutes. The rapid heating rate and superheating/"hot spots" of the reaction system under microwave irradiation result in a large amount of nuclei in a short time, leading to the formation of a large number of clusters. The clusters grow up rapidly and assemble into TiO_2 nanocrystallite aggregates. The TiO_2 aggregates show better light scattering properties, larger specific surface area and higher dye-loading than those of the commercial P25 TiO_2 nanoparticles. In comparison with P25, the short current density (J_{sc}) and dye-loading of DSC based the as-synthesized TiO_2 aggregates increase by 33% and 62%, respectively. As a result, the PCE of the DSC is up to 7.64%.

Acknowledgements

This work was supported by the National Science Foundation of China (51374029), the Program for New Century Excellent Talents in University (NCET-13-0668) and the Fundamental Research Funds for the Central Universities (FRF-TP-14-008C1). This work was also supported by the "thousands talents" program for pioneer researcher and his innovation team, China.

Notes and references

1 E. J. W. Crossland, N. Noel, V. Sivaram, T. Leijtens, J. A. Alexander-Webber and H. J. Snaith, *Nature*, 2013, **495**, 215–219.
2 J. S. Chen, Y. L. Tan, C. M. Li, Y. L. Cheah, D. Y. Luan, S. Madhavi, F. Y. C. Boey, L. A. Archer and X. W. Lou, *J. Am. Chem. Soc.*, 2010, **132**, 6124–6130.
3 B. Oregan and M. Gratzel, *Nature*, 1991, **353**, 737–740.
4 C. J. Barbe, F. Arendse, P. Comte, M. Jirousek, F. Lenzmann, V. Shklover and M. Gratzel, *J. Am. Ceram. Soc.*, 1997, **80**, 3157–3171.
5 M. K. Nazeeruddin, P. Pechy, T. Renouard, S. M. Zakeeruddin, R. Humphry-Baker, P. Comte, P. Liska, L. Cevey, E. Costa, V. Shklover, L. Spiccia, G. B. Deacon, C. A. Bignozzi and M. Gratzel, *J. Am. Chem. Soc.*, 2001, **123**, 1613–1624.
6 R. Gao, L. Wang, Y. Geng, B. Ma, Y. Zhu, H. Dong and Y. Qiu, *J. Phys. Chem. C*, 2011, **115**, 17986–17992.
7 R. Gao, L. Wang, B. Ma, C. Zhan and Y. Qiu, *Langmuir*, 2010, **26**, 2460–2465.
8 T. Kinoshita, J. T. Dy, S. Uchida, T. Kubo and H. Segawa, *Nat. Photonics*, 2013, **7**, 535–539.
9 K. Lee, S. W. Park, M. J. Ko, K. Kim and N. G. Park, *Nat. Mater.*, 2009, **8**, 665–671.
10 J.-Y. Liao, J.-W. He, H. Xu, D.-B. Kuang and C.-Y. Su, *J. Mater. Chem.*, 2012, **22**, 7910–7918.
11 S. Mathew, A. Yella, P. Gao, R. Humphry-Baker, B. F. E. Curchod, N. Ashari-Astani, I. Tavernelli, U. Rothlisberger, M. K. Nazeeruddin and M. Graetzel, *Nat. Chem.*, 2014, **6**, 242–247.
12 X. Feng, K. Zhu, A. J. Frank, C. A. Grimes and T. E. Mallouk, *Angew. Chem.*, 2012, **51**, 2727–2730.
13 Y. J. Kim, M. H. Lee, H. J. Kim, G. Lim, Y. S. Choi, N.-G. Park, K. Kim and W. I. Lee, *Adv. Mater.*, 2009, **21**, 3668–3673.
14 J. Wang and Z. Lin, *Chem. Mater.*, 2008, **20**, 1257–1261.
15 M. D. Ye, X. K. Xin, C. J. Lin and Z. Q. Lin, *Nano Lett.*, 2011, **11**, 3214–3220.
16 J. Lin, Y. U. Heo, A. Nattestad, Z. Sun, L. Wang, J. H. Kim and S. X. Dou, *Sci. Rep.*, 2014, **4**, 5769.
17 R. Gao, J. Tian, Z. Liang, Q. Zhang, L. Wang and G. Cao, *Nanoscale*, 2013, **5**, 1894–1901.
18 W. Wang, H. Zhang, R. Wang, M. Feng and Y. Chen, *Nanoscale*, 2014, **6**, 2390–2396.
19 R. Gao, Z. Liang, J. Tian, Q. Zhang, L. Wang and G. Cao, *Nano Energy*, 2013, **2**, 40–48.

20 T. P. Chou, Q. F. Zhang, G. E. Fryxell and G. Z. Cao, *Adv. Mater.*, 2007, **19**, 2588–2592.
21 J. Xi, Q. Zhang, K. Park, Y. Sun and G. Cao, *Electrochim. Acta*, 2011, **56**, 1960–1966.
22 Q. F. Zhang, T. R. Chou, B. Russo, S. A. Jenekhe and G. Z. Cao, *Angew. Chem., Int. Ed.*, 2008, **47**, 2402–2406.
23 Q. Zhang, E. Uchaker, S. L. Candelaria and G. Cao, *Chem. Soc. Rev.*, 2013, **42**, 3127–3171.
24 Q. F. Zhang and G. Z. Cao, *Nano Today*, 2011, **6**, 91–109.
25 Q. F. Zhang and G. Z. Cao, *J. Mater. Chem.*, 2011, **21**, 6769–6774.
26 M. J. Alam and D. C. Cameron, *J. Sol-Gel Sci. Technol.*, 2002, **25**, 137–145.
27 K.-i. Katsumata, Y. Ohno, K. Tomita, T. Taniguchi, N. Matsushita and K. Okada, *ACS Appl. Mater. Interfaces*, 2012, **4**, 4846–4852.
28 C.-T. Dinh, T.-D. Nguyen, F. Kleitz and T.-O. Do, *ACS Nano*, 2009, **3**, 3737–3743.
29 T. R. Gordon, M. Cargnello, T. Paik, F. Mangolini, R. T. Weber, P. Fornasiero and C. B. Murray, *J. Am. Chem. Soc.*, 2012, **134**, 6751–6761.
30 I. Bilecka and M. Niederberger, *Nanoscale*, 2010, **2**, 1358–1374.
31 M. I. Dar, A. K. Chandiran, M. Gratzel, M. K. Nazeeruddin and S. A. Shivashankar, *J. Mater. Chem. A*, 2014, **2**, 1662–1667.
32 K. Manseki, Y. Kondo, T. Ban, T. Sugiura and T. Yoshida, *Dalton Trans.*, 2013, **42**, 3295–3299.
33 K. F. Moura, J. Maul, A. R. Albuquerque, G. P. Casali, E. Longo, D. Keyson, A. G. Souza, J. R. Sambrano and I. M. G. Santos, *J. Solid State Chem.*, 2014, **210**, 171–177.
34 Asdim, K. Manseki, T. Sugiura and T. Yoshida, *New J. Chem.*, 2014, **38**, 598–603.
35 P.-S. Shen, Y.-C. Tai, P. Chen and Y.-C. Wu, *J. Power Sources*, 2014, **247**, 444–451.
36 M. Cargnello, T. R. Gordon and C. B. Murray, *Chem. Rev.*, 2014, **114**, 9319–9345.
37 A. R. Tao, S. Habas and P. D. Yang, *Small*, 2008, **4**, 310–325.
38 G. Cao and Y. Wang, *Nanostructures and Nanomaterials*, World Scientifics Publishing Co. Pte. Ltd., Singapore, 2011, pp. 45–46.
39 Y. J. Zhu and F. Chen, *Chem. Rev.*, 2014, **114**, 6462–6555.
40 Q. Zhang, D. Myers, J. Lan, S. A. Jenekhe and G. Cao, *Phys. Chem. Chem. Phys.*, 2012, **14**, 14982–14998.
41 J. Tian, L. Lv, X. Wang, C. Fei, X. Liu, Z. Zhao, Y. Wang and G. Cao, *J. Phys. Chem. C*, 2014, **118**, 16611–16617.
42 N. A. Dahoudi, J. Xi and G. Cao, *Electrochim. Acta*, 2012, **59**, 32–38.
43 Y. Shi, K. Wang, Y. Du, H. Zhang, J. Gu, C. Zhu, L. Wang, W. Guo, A. Hagfeldt, N. Wang and T. Ma, *Adv. Mater.*, 2013, **25**, 4413–4419.
44 J. Bisquert, F. Fabregat-Santiago, I. Mora-Sero, G. Garcia-Belmonte and S. Gimenez, *J. Phys. Chem. C*, 2009, **113**, 17278–17290.
45 P. Chen, J. H. Yum, F. De Angelis, E. Mosconi, S. Fantacci, S.-J. Moon, R. H. Baker, J. Ko, M. K. Nazeeruddin and M. Graetzel, *Nano Lett.*, 2009, **9**, 2487–2492.
46 B. Liu, X. Wang, L. Wen and X. Zhao, *Chem.–Eur. J.*, 2013, **19**, 10751–10759.
47 J. J. Tian, R. Gao, Q. F. Zhang, S. G. Zhang, Y. W. Li, J. L. Lan, X. H. Qu and G. Z. Cao, *J. Phys. Chem. C*, 2012, **116**, 18655–18662.